Chemical Science

ROYAL SOCIETY OF CHEMISTRY

EDGE ARTICLE

View Article Online
View Journal | View Issue



Cite this: *Chem. Sci.*, 2023, **14**, 2070

All publication charges for this article have been paid for by the Royal Society of Chemistry

Received 10th November 2022
Accepted 16th January 2023

DOI: 10.1039/d2sc06209g

rsc.li/chemical-science



# Two birds one stone: β-fluoropyrrolyl-cysteine $S_NAr$ chemistry enabling functional porphyrin bioconjugation†

Guo-Qing Jin,[a] Jing-Xiang Wang,[a] Jianhua Lu,[a] Hang Zhang,[a] Yuhang Yao,[a] Yingying Ning,[a] Hua Lu,[a] Song Gao[abc] and Jun-Long Zhang *[ab]

Bioconjugation, a synthetic tool that endows small molecules with biocompatibility and target specificity through covalent attachment of a biomolecule, holds promise for next-generation diagnosis or therapy. Besides the establishment of chemical bonding, such chemical modification concurrently allows alteration of the physicochemical properties of small molecules, but this has been paid less attention in designing novel bioconjugates. Here, we report a "two birds one stone" methodology for irreversible porphyrin bioconjugation based on β-fluoropyrrolyl-cysteine $S_NAr$ chemistry, in which the β-fluorine of porphyrin is selectively replaced by a cysteine in either peptides or proteins to generate novel β-peptidyl/proteic porphyrins. Notably, due to the distinct electronic nature between fluorine and sulfur, such replacement makes the Q band red-shift to the near-infrared region (NIR, >700 nm). This facilitates intersystem crossing (ISC) to enhance the triplet population and thus singlet oxygen production. This new methodology features water tolerance, a fast reaction time (15 min), good chemo-selectivity, and broad substrate scope, including various peptides and proteins under mild conditions. To demonstrate its potential, we applied porphyrin β-bioconjugates in several scenarios, including (1) cytosolic delivery of functional proteins, (2) metabolic glycan labeling, (3) caspase-3 detection, and (4) tumor-targeting phototheranostics.

## Introduction

Bioconjugation represents an innovative synthetic strategy allowing the complementary usage of both chemical and biological approaches to construct functional molecules.[1,2] Toward this goal, a number of efficient and selective bioconjugations have been discovered over the decades and have succeeded in attaching small molecules to biomolecules of interest (*e.g.*, peptide, protein, nucleic acid, or carbohydrate) *via* a covalent bond.[3–8] In most cases, such modification is assumed not to affect the intrinsic properties of the small molecules. However, as a matter of fact, any formation of a new bond more or less perturbs the electronic nature of the small molecule and even influences its physicochemical properties and functions. To date, it is still far from well recognized that a significant opportunity exists in implementing bioconjugation: that is, to tailor the structural and functional diversity of small molecules beyond establishing a robust connection with biomolecules.[9–11] Such recognition is particularly relevant to fabricating porphyrin bioconjugates for diagnostic or therapeutic purposes, as described in this work.

Porphyrin and its derivatives are time-honoured photosensitizers that share a similar tetrapyrrole core to naturally occurring light-harvesting antennas and redox cofactors, with extensive applications in functional materials, catalysis, and biomedicines.[12–17] As artificial synthetic macrocycles, they are subject to chemical manipulation to create desirable "drug-like" entities featuring structural diversity. Biomolecules, such as oligonucleotides,[18,19] peptides,[20] proteins,[21] and carbohydrates[12,22] have been used to endow synthetic porphyrins with biocompatibility and tumour-specificity. Among them, *meso*-aryl groups have mainly been chosen as conjugation sites due to lower steric hindrance and the rich synthetic repertoire of aryl groups. However, *meso*-aryl is perpendicular to the tetrapyrrolic plane and hardly delivers electronic engagement in π-conjugation and the related excited states. In contrast, fine-tuning of the π-periphery enables facile, efficient modulation of photophysical properties, but an efficient and selective β-bioconjugation approach has not been achieved due to peripherial

[a]*Beijing National Laboratory for Molecular Sciences, College of Chemistry and Molecular Engineering, Peking University, Beijing 100871, P. R. China. E-mail: zhangjunlong@pku.edu.cn*

[b]*Chemistry and Chemical Engineering Guangdong Laboratory, Shantou 515031, P. R. China*

[c]*Spin-X Institute, School of Chemistry and Chemical Engineering, State Key Laboratory of Luminescent Materials and Devices, Guangdong-Hong Kong-Macao Joint Laboratory of Optoelectronic and Magnetic Functional Materials, South China University of Technology, Guangzhou 510641, China*

† Electronic supplementary information (ESI) available. See DOI: https://doi.org/10.1039/d2sc06209g

steric hindrance and relatively inert reactivity. To fill the knowledge gap, we aimed to develop a general approach toward functional porphyrin β-bioconjugates with better perceived photophysical properties.

Sulfur, often embodied in cysteine, plays an important role in post-translational and site-selective bioconjugation owing to its relatively low abundance in proteins and inherently high nucleophilicity.[23–26] Through the rational design of electrophilic warheads such as maleimides,[27] a new irreversible C–S bond typically formed with a cysteine residue has been extensively exploited in designing bio-probes,[28] small molecule inhibitors,[29] and antibody–drug conjugates.[30] However, the β-pyrrolic ring in porphyrins is not electrophilic enough to react with cysteine under physiological conditions. To increase their electrophilicity, pioneering work has demonstrated that the fluorination of aromatics enhances their reactivity, namely fluorine-cysteine $S_NAr$ chemistry by Pentelute,[31] Derda,[32] Diness,[33] and Harran[34] (Fig. 1). This was ascribed to the highest electronegativity of fluorine among all elements in the periodic table, which increases the electrophilicity of the neighbouring carbon in perfluoroarenes[31–33] and octafluorocyclopentenes[34] so as to react with a cysteine residue.[35] In the contest for porphyrin bioconjugates, fluorine-thiol replacement at the *meso*-pentafluorophenyl group with thiosugars[22] or sulfhydryl-terminated polyethylene glycol[36] has been explored to improve biocompatibility, but such conjugation seldom altered photophysical properties. Thus, exploiting a new synthetic modification at the π-periphery is of importance to simultaneously achieve biocompatibility and tailor photophysical properties.

An anticipated bonus for such fluorine-thiol exchange at the β-periphery is manipulation of the excited states and related photophysical properties arising from the distinct electronic nature between fluorine and sulfur.[37–39] As a manifestation of β-fluoropyrrolyl-cysteine $S_NAr$ chemistry, we first performed computational calculations to predict the photophysical properties before and after β-fluorine-thiol replacement. We then prepared a series of water-soluble β-octafluoroporphyrins and investigated β-fluorine-thiol replacement with peptides/proteins under physiological conditions (Fig. 1). To our delight, β-peptidyl porphyrins were obtained quickly (15 min) and selectively (mono-peptidyl conjugates) with good yields (80–99%). As predicted by the computational calculations, the obtained β-peptidyl porphyrins displayed a bathochromic shift of the porphyrinic Q band to the NIR region and population of triplet states in favour of ROS generation that has been validated to develop tumour-targeted photosensitizers. Finally, we demonstrated several potential application scenarios, including (1) cytosolic delivery of functional proteins, (2) metabolic glycan labeling, (3) caspase-3 detection, and (4) tumour-targeting phototheranostics. Therefore, given that the importance of

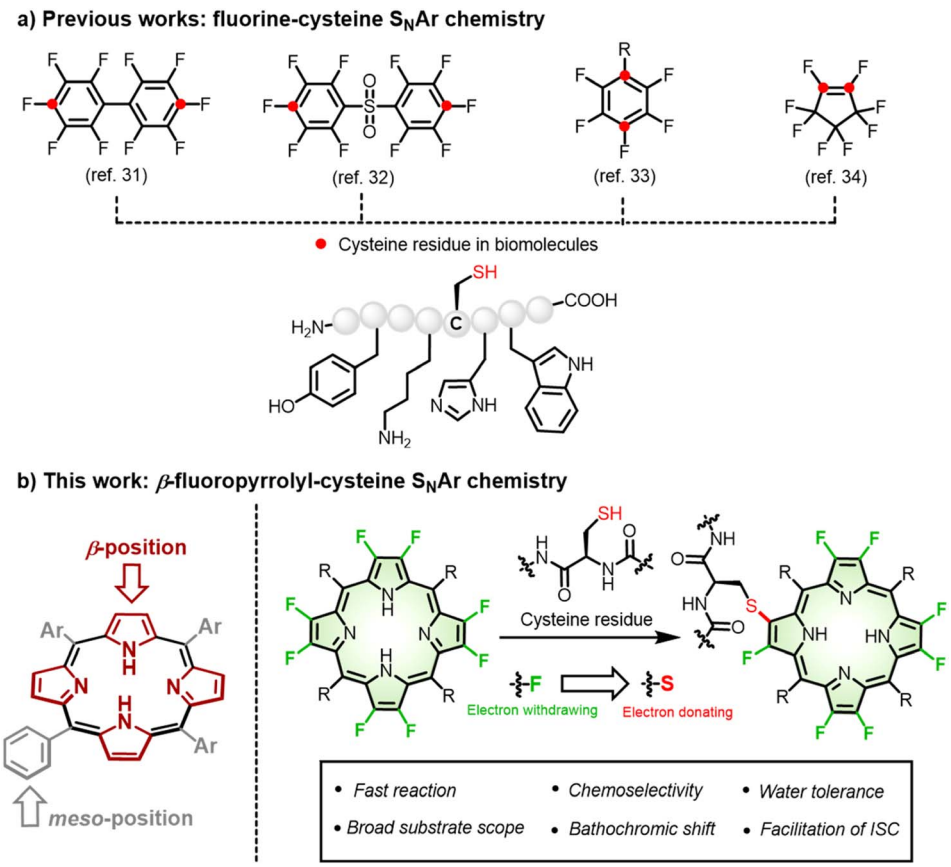


Fig. 1 (a) Reported fluorine-cysteine replacement chemistry and corresponding reactive sites (red) of perfluoro-reagents. (b) β-fluoropyrrolyl-cysteine $S_NAr$ chemistry for irreversible porphyrin bioconjugation.

porphyrins and their derivatives in biological studies and biomedicines, the synthetic approach described here provided generally feasible access to endow biocompatibility, tumour specificity, and tunable photophysical properties.

## Results and discussion

### Computational studies

To predict the photophysical properties of porphyrins after β-fluorine-thiol replacement, we performed density functional theory (DFT) and time-dependent DFT (TDDFT) calculations based on 2,3,7,8,12,13,17,18-octafluoro-5,10,15,20-tetrakisphenyl porphyrin (**P$_1$**) and β-sulfur substituted porphyrins (**P$_2$** and **P$_3$**). The energy diagram and the corresponding nodal patterns of the frontier molecular orbitals (FMOs) are shown in Fig. 2. The first singlet excited states ($S_1$ states) of **P$_{1-3}$** were mainly attributed to the $a_{2u} \rightarrow e_g^*$ transition. β-Fluorine-thiol replacement introduced interference from the anti-bonding orbitals of the sulfur atoms, destabilizing the energy level of the HOMO (highest occupied molecular orbital). Hence, the energy gaps between HOMO and LUMO (lowest unoccupied molecular orbital) for **P$_{1-3}$** decreased in the order of **P$_1$** (2.8 eV) > **P$_2$** (2.64 eV) > **P$_3$** (2.58 eV) as replacement of the β-sulfur atom increased, indicating gradually red-shifted absorption. On the other hand, the anti-bonding orbitals of the sulfur atoms effectively stabilized the energy level of low-lying triplet states ($T_n$ states). As shown in Table S5,† there were three triplet states ($T_1$–$T_3$) below the $S_1$ state of **P$_2$** or **P$_3$**, while only two nearly degenerate triplet states ($T_1$–$T_2$) existed below the $S_1$ state of unsubstituted **P$_1$**.

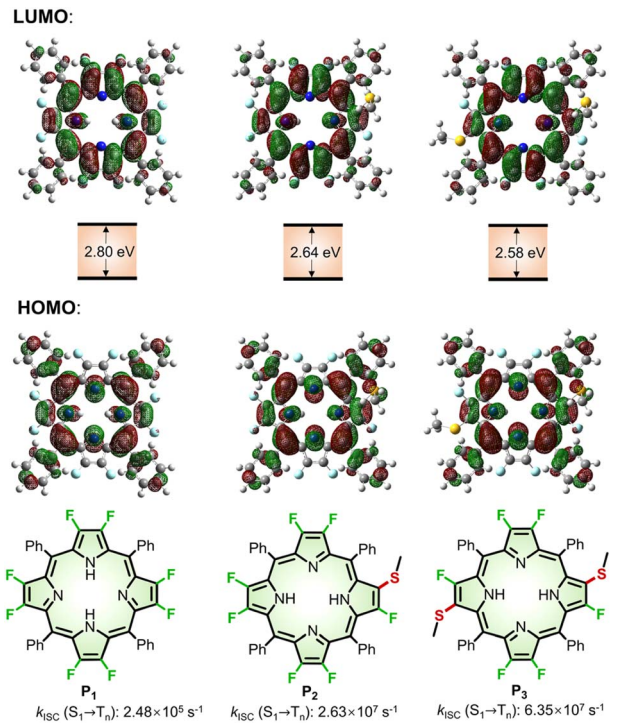


Fig. 2 Nodal patterns of the frontier molecular orbitals (FMOs), HOMO–LOMO energy gaps, and $k_{ISC}$ for ($S_1 \rightarrow T_n$) of **P$_{1-3}$** based on DFT and TDDFT calculations.

We theoretically explored the dynamics of the excited states, including spin–orbit coupling (SOC) constants and intersystem crossing (ISC) rates before and after β-fluorine-thiol replacement. As a result, the SOC constants significantly increased from 0.0418 $cm^{-1}$ (**P$_1$**) to 0.604 $cm^{-1}$ (**P$_2$**) and 1.26 $cm^{-1}$ (**P$_3$**) and the singlet–triplet energy gap ($\Delta E_{S\text{-}T}$) decreased from 1.24 eV (**P$_1$**) to 0.0432 eV (**P$_2$**) and 0.0405 eV (**P$_3$**) after β-fluorine-thiol exchange, leading to a tremendous enhancement of the ISC rate constants ($k_{ISC}$) from the $S_1$ to the $T_n$ state. In particular, as the number of β-sulfur atoms increased, the $k_{ISC}$ ($S_1 \rightarrow T_n$) of $2.63 \times 10^7$ $s^{-1}$ (**P$_2$**) and $6.35 \times 10^7$ $s^{-1}$ (**P$_3$**) were estimated to be 2 orders of magnitude higher than $2.48 \times 10^5$ $s^{-1}$ (**P$_1$**). Therefore, these computational results encouraged us to exploit β-fluoropyrrolyl-cysteine $S_NAr$ chemistry in pursuit of porphyrin bioconjugates with red-shifted absorption and accelerated ISC processes.

### Optimizing the reaction condition

To optimize the reaction condition (Fig. 3a), we started with bioconjugation between **P$_4$** and glutathione (GSH, **a**), the most abundant tripeptide in living cells.[40] As displayed in Table 1, entry 1, the reaction between **P$_4$** (1 mM) and **a** (2 mM) in Tris buffer (pH 8.0) for 15 min afforded β-peptidyl porphyrins with a yield of 68%. High-performance liquid chromatography (HPLC) analysis (Fig. S2–S11†) showed mono- (**P$_4$-a**) and di-peptidyl porphyrins (**P$_4$-2a**), as displayed in a ratio of 87 : 13 (Table 1, entry 1). Daylight had a trivial effect on β-bioconjugation (Table 1, entry 2). By decreasing GSH concentrations (Table 1, entries 3–6), mono-peptidyl porphyrins (**P$_4$-a**) (>99% yield) were selectively obtained after β-fluorine-cysteine replacement (Table 1, entry 6). Inspired by a reported reaction-optimizing strategy by tuning the ratio of reactants,[41,42] here largely excessive β-octafluoroporphyrin (4 equivalents) could effectively facilitate intermolecular $S_NAr$ replacement between porphyrin and GSH to achieve mono-substitution. A shortened reaction time (5 min) lowered the yield to 58% (Table 1, entry 7). Otherwise, when the reaction process was prolonged to 30 min, more di-substituted products were observed (13%, Table 1, entry 8). Increasing the pH to 8.8 led to a moderate yield of 59% (Table 1, entry 9). In contrast, lowering the pH to 7.4 gave a lower yield (46%) with **P$_4$-a** as the dominant product (Table 1, entry 10). Next, we measured the reaction rates using the model reaction between **P$_4$** and **a** in Tris buffer (pH 8.0), which gave a rate constant of 1.44 $M^{-1}$ $s^{-1}$ according to the time-course study (Fig. S12, see details in the "Methods" part of ESI†).

As the intracellular GSH concentration was 2–10 mM,[43] we evaluated the stability of **P$_4$-a** in GSH-abundant media (10 mM, pH 7.4, 37 °C) within 24 h (Fig. S13†). 67% of **P$_4$-a** remained intact under such conditions. According to HPLC analysis, multi-substituted conjugates were formed, suggesting that **P$_4$-a** partially reacts with GSH. However, such reactivity was inhibited when the pH was lowered to 6.8. After 24 h, **P$_4$-a** was totally recovered, indicating the reaction was pH-sensitive, and that **P$_4$-a** may remain intact in an acidic microenvironment, for

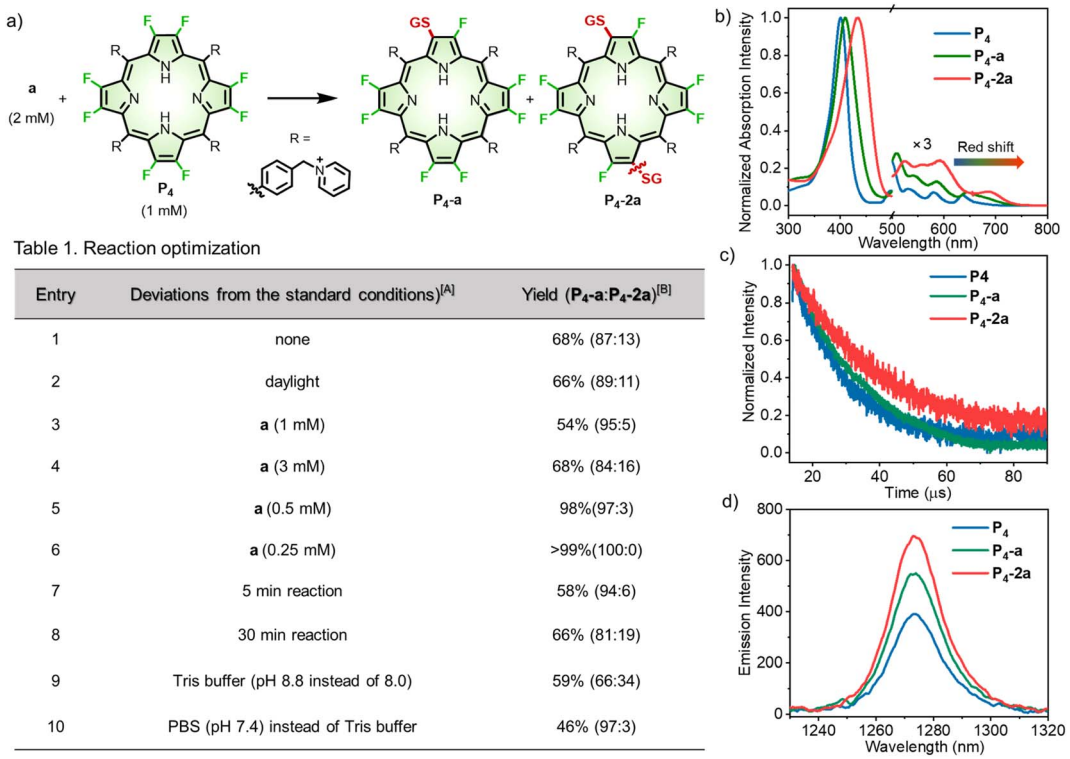


Table 1. Reaction optimization

| Entry | Deviations from the standard conditions)[A] | Yield (**P$_4$-a**:**P$_4$-2a**)[B] |
|---|---|---|
| 1 | none | 68% (87:13) |
| 2 | daylight | 66% (89:11) |
| 3 | **a** (1 mM) | 54% (95:5) |
| 4 | **a** (3 mM) | 68% (84:16) |
| 5 | **a** (0.5 mM) | 98%(97:3) |
| 6 | **a** (0.25 mM) | >99%(100:0) |
| 7 | 5 min reaction | 58% (94:6) |
| 8 | 30 min reaction | 66% (81:19) |
| 9 | Tris buffer (pH 8.8 instead of 8.0) | 59% (66:34) |
| 10 | PBS (pH 7.4) instead of Tris buffer | 46% (97:3) |

Fig. 3 (a) Reaction optimization. [A] Standard conditions: **a** (2 mM) and **P$_4$** (1 mM) reacted in Tris buffer (pH 8.0) at room temperature in the dark for 15 min. [B] The yields were determined according to calibrated HPLC integral areas. (b) Normalized UV-visible absorption spectra of **P$_4$**, **P$_4$-a** and **P$_4$-2a** in methanol. (c) The excited state lifetime decay curves of **P$_4$**, **P$_4$-a** and **P$_4$-2a** in degassed methanol. (d) NIR emission of $^1O_2$ at 1270 nm excited at 410 nm in toluene (0.1% DMSO).

example, tumors.[43,44] To demonstrate the cell stability of **P$_4$-a**, we treated HeLa cells with **P$_4$-a** (10 μM) for different time periods. After the treatment, the HeLa cells were lysed using RIPA (Radio-Immunoprecipitation Assay) lysis buffer, then analysed by HPLC and sulfate polyacrylamide gel electrophoresis (SDS-PAGE). HPLC analysis for each cell lysate displayed the peak of **P$_4$-a** alone, indicating **P$_4$-a** did not react with cysteine-containing biomolecules in HeLa cells (Fig. S14†). Furthermore, SDS-PAGE analysis of the cell lysate showed no fluorescence from **P$_4$-a** and Coomassie brilliant blue (CBB)-stained gel showed no molecular weight increases (Fig. S15†). These results also demonstrated no reaction between **P$_4$-a** and cysteine-containing proteins; thus **P$_4$-a** displayed good chemical stability in cells.

## Photophysical properties

We then investigated the photophysical properties of **P$_4$**, **P$_4$-a**, and **P$_4$-2a**. After the β-fluorine-sulfur replacement, the Soret band (401 nm) of **P$_4$** red-shifted to 409 nm and 433 nm for **P$_4$-a** and **P$_4$-2a**, respectively (Fig. 3b). Importantly, the Q bands of **P$_4$-a** and **P$_4$-2a** extended to 716 and 736 nm with remarkable red-shifts of 41 and 61 nm compared to **P$_4$** (675 nm). The bathochromic absorption after β-fluorine-sulfur replacement was consistent with that obtained in the computational studies. To the best of our knowledge, any known bioconjugation at *meso*-positions has not been reported to induce such large red-shifted Q-bands.[21] By performing nanosecond transient absorption, the triplet decays for **P$_4$**, **P$_4$-a**, and **P$_4$-2a** were determined to be 14, 19, and 24 μs in degassed methanol, respectively (Fig. 3c). The remarkably prolonged triplet lifetimes of **P$_4$-a** and **P$_4$-2a** compared to **P$_4$** revealed that β-fluoropyrrolyl-cysteine $S_NAr$ chemistry facilitated the intersystem crossing (ISC) process and enhanced the population of triplet state as well as the efficiency of oxygen sensitization, arising from the heavy atom effect of sulfur.[45] Accordingly, the NIR emission of singlet oxygen ($^1O_2$) at 1270 nm upon irradiation of **P$_4$**, **P$_4$-a**, and **P$_4$-2a** increased gradually with the extent of sulfur replacement (Fig. 3d). The quantum yields ($\Phi_\Delta$s) of singlet oxygen were determined in toluene using the comparative method referenced to TPP, as 75%, 84%, and 92% for **P$_4$**, **P$_4$-a**, and **P$_4$-2a** (Fig. S16†). Furthermore, we examined the cell cytotoxicity of **P$_4$**, **P$_4$-a**, and **P$_4$-2a** in the absence or presence of light (Fig. S17 and S18†). The photocytotoxicity, represented by the half-maximal inhibitory concentrations ($IC_{50}$s) for **P$_4$** (1.97 ± 0.06 μM), **P$_4$-a** (0.95 ± 0.03 μM), and **P$_4$-2a** (0.51 ± 0.01 μM), was obtained under irradiation (LED laser (400–700 nm), 10 mW cm$^{-2}$, 10 min). The results showed that β-sulfur substitution enhanced the $^1O_2$-induced photocytotoxicity but slightly affected the dark cytotoxicity.

## Peptide scopes

Several amino acid residues possessed intrinsic nucleophilic reactivity toward C–F bonds; we investigated the cysteine-

selectivity among the nucleophilic residues using $\mathbf{P_4}$ as a porphyrin substrate (Scheme 1). Peptide **b** containing several nucleophilic amino-acids (Cys, Ser, Lys, His, Arg, and Trp) was designed and used. In the context, we conducted the β-fluoropyrrolyl-cysteine $S_NAr$ reaction according to the reaction conditions (Table 1, entry 6). The reaction of $\mathbf{P_4}$ with **b** in Tris buffer (pH 8.0) for 15 min afforded conjugate $\mathbf{P_4}$-**b** in a yield of 90% (Fig. S19†). As a control, when iodoacetamide (**IAA**) was used to specifically block the cysteine of **b**, the subsequent addition of $\mathbf{P_4}$ could not give the $\mathbf{P_4}$-**b** product even after 24 h, indicating that conjugation of $\mathbf{P_4}$-**b** occurred at the cysteine residue. Encouraged by these preliminary results, we examined various peptides with cysteine at different positions (Fig. S20–S24†), including N- (**c**)/C-terminus (**d**), the middle of peptide (**e**), and cyclic peptide (**f**). Peptides **c–f** with hydrophobic and steric phenyl or isopropyl groups could efficiently conjugate with $\mathbf{P_4}$ *via* β-fluorine-cysteine substitution and gave mono-peptidyl products in 68–99% yields. Of note, the biotinylated peptide (**g**) could react with $\mathbf{P_4}$ to afford $\mathbf{P_4}$-**g** in 99% yield.

## Porphyrin scopes

On the other hand, to investigate the scope of porphyrins, we employed GSH as a model peptide under the optimized reaction conditions (Fig. S25–S32†). As shown in Scheme 2a, we used three types of β-octafluoroporphyrins containing cationic, anionic, and neutral *meso*-aryl groups, respectively. We found that, with the modification of pyridinium ($\mathbf{P_4}$), quaternary ammonium ($\mathbf{P_{5-9}}$), phosphonium ($\mathbf{P_{10}}$), or sulfonium ($\mathbf{P_{11}}$) cations, β-octafluoroporphyrins showed high reactivity toward GSH with yields of 83–99% (mono-peptidyl conjugates). Due to poor water solubility or steric hindrance, the PEGylated porphyrin ($\mathbf{P_{12}}$) could not conjugate with GSH under such reaction conditions. By adding dimethyl sulfoxide (DMSO) to facilitate the solubility of $\mathbf{P_{12}}$ (see details in the Methods part of ESI†), β-fluoropyrrolyl-cysteine replacement progressed smoothly with 80% yield of $\mathbf{P_{12}}$-**a** (Fig. S33†). The negatively charged sulfonate porphyrin ($\mathbf{P_{13}}$) also reacted with GSH in a complete conversion (>99%) monitored by UV-visible absorption (Fig. S34†), but the products could not be isolated under the HPLC conditions described above (see details in the "Methods" part of ESI†). High-resolution mass spectrometry (HRMS) confirmed the corresponding molecular weights of the formed conjugate $\mathbf{P_{13}}$-**a** (Fig. S35†).

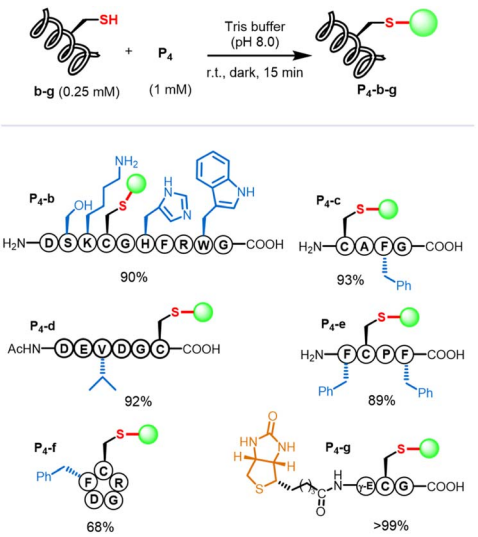


Scheme 1 Scope of peptides. Reaction conditions: peptides **b-g** (0.25 mM) and $P_4$ (1 mM) reacted in Tris buffer (pH 8.0) at room temperature in the dark for 15 min. The yield was determined according to calibrated HPLC integral areas of $P_4$-**b-g**.

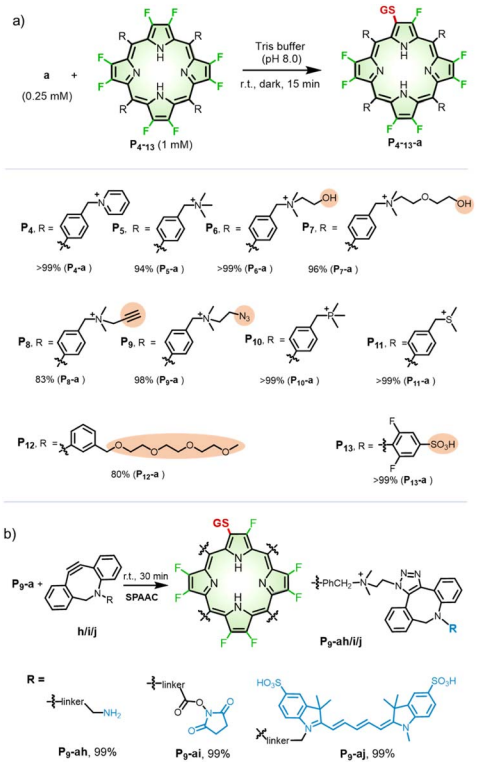


Scheme 2 (a) Scope of β-octafluoroporphyrins. Reaction conditions: **a** (0.25 mM) and $P_{4-13}$ (1 mM) in Tris buffer (pH 8.0) at room temperature in the dark for 15 min. For $P_{12-13}$, the reaction conditions were partially changed, as described in the "Methods" part of ESI.† The yield was determined according to calibrated HPLC integral areas of $P_{4-12}$-**a**. (b) SPAAC reaction of $P_9$-**a** with DBCO derivatives (**h–j**).

Note that, to test whether the β-fluoropyrrolyl-cysteine $S_NAr$ reaction was compatible with other bioconjugations such as Click chemistry,[46] we used alkynyl ($\mathbf{P_8}$) or azido ($\mathbf{P_9}$) β-octafluoroporphyrin as the substrate to conjugate with GSH, which gave $\mathbf{P_8}$-**a** (83%) and $\mathbf{P_9}$-**a** (98%), respectively, as shown in Scheme 2a. To reveal the potential of multi-functionalization, we carried out a bioorthogonal strain-promoted alkyne–azide cycloaddition (SPAAC)[47] between azido β-peptidyl porphyrin ($\mathbf{P_9}$-**a**) and dibenzocyclooctyne derivatives (DBCO, **h–j**), as shown in Scheme 2b. Specifically, $\mathbf{P_9}$-**a** was mixed and reacted with sulfo-DBCO-amine (**h**), DBCO-PEG4-NHS (**i**), or disulfo-Cy5-DBCO (**j**) in water for 30 min. These reactions afforded $\mathbf{P_9}$-**ah**, $\mathbf{P_9}$-**ai**, or $\mathbf{P_9}$-**aj**, respectively, whose molecular weights were confirmed by HRMS, in quantitative yields, as determined by HPLCs (Fig. S36–S38†). Therefore, we demonstrated the compatibility

of the β-fluoropyrrolyl-cysteine $S_NAr$ reaction with Click chemistry that helps to establish porphyrin as a molecular platform with multiple functions.

### Protein conjugation

We next extended the reaction to protein conjugation. Here, an enhanced green fluorescent protein (EGFP) with a genetically introduced cysteine[48] was chosen as the model protein. We conducted the bioconjugation following the synthetic procedure shown in Fig. 4a (see details in the "Methods" part of ESI†). Firstly, EGFP (50 μM) was mixed with **$P_4$** (1 mM, 20 equiv.) in Tris buffer (pH 8.0) at room temperature for 8 hours. As shown in Fig. 4b, the mass peak (Obs. 30 436 Da) of **$P_4$-EGFP**, consistent with the calculated molecular weight (Cal. 30 437 Da), was obtained with a mass spectrometer. As a control, when the cysteine residue in EGFP was blocked by excess **IAA** before reacting with **$P_4$**, no **$P_4$-EGFP** was observed but **IAA-EGFP** (Fig. S39†) alone. Similarly, conjugation of EGFP with **$P_8$** or **$P_{13}$** gave **$P_8$-EGFP** or **$P_{13}$-EGFP**. As shown in Fig. 4c, SDS-PAGE analysis showed that EGFP converted into the corresponding conjugates in >95% yield. Thus, either the positively or negatively charged β-octafluoroporphyrin could effectively conjugate with EGFP.

We conducted fluorescence scanning for the same SDS-PAGE gel before CBB-staining (Fig. 4c). All porphyrin conjugates showed the red fluorescence attributed to porphyrin. In PBS (pH = 7.4) solution, **$P_4$-EGFP** showed the characteristic UV-visible absorption of EGFP and **$P_4$** (Fig. 4d). Upon 450 nm excitation, it displayed two emission bands at 480–600 and 620–800 nm, assigned to the fluorescence of EGFP and **$P_4$**, respectively (Fig. 4e).

Serum albumin is abundant in blood plasma, containing a free cysteine residue (cysteine 34),[49] and it plays important roles in biomedical applications.[43,50] When bovine serum albumin (BSA) was used, the observed mass peaks (67 634 Da for **$P_4$-BSA** and 67 729 Da for **$P_{13}$-BSA**) were obtained, consistent with the calculated values. This indicated BSA was modified with a single porphyrin (Fig. 4f). SDS-PAGE analysis showed

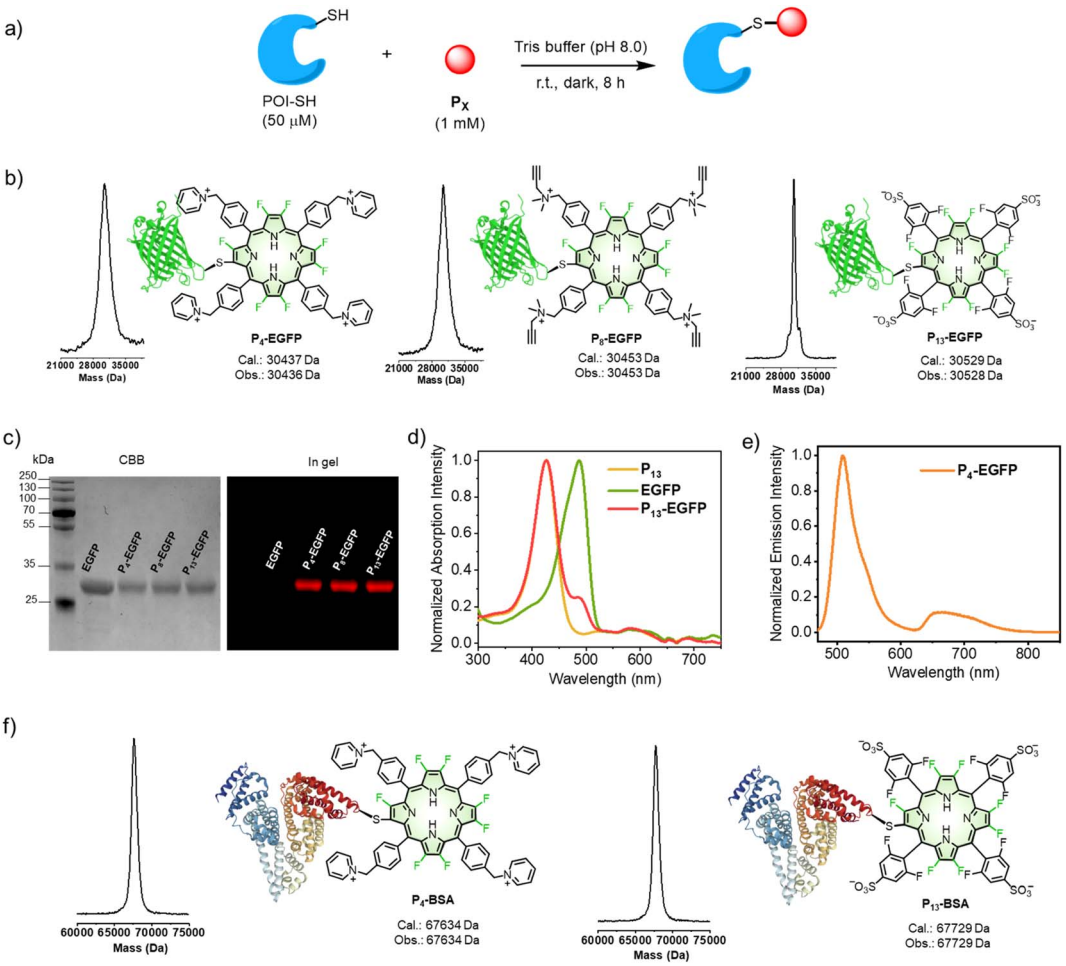


Fig. 4 (a) β-Fluoropyrrolyl-cysteine $S_NAr$ chemistry for cysteine-selective bioconjugation of a protein of interest (POI). (b) Mass spectra of synthetic porphyrin–EGFP conjugates. Cal. (calculated mass); Obs. (observed mass). (c) SDS-PAGE of β-fluoropyrrolyl-cysteine $S_NAr$ reaction mixtures between EGFP and $P_4$/$P_8$/$P_{13}$. The Coomassie brilliant blue (CBB)-stained gel showed increased protein weights. In-gel fluorescence scanning showed porphyrin emission (red). (d) UV-visible absorption spectra of $P_4$, EGFP, and **$P_4$-EGFP** in 1× PBS (pH = 7.4). (e) Fluorescence emission spectrum of **$P_4$-EGFP** in 1× PBS (pH = 7.4). $\lambda_{ex}$ = 450 nm. (f) Mass spectra of synthetic porphyrin–BSA conjugates.

increased molecular weights (CBB staining) compared with BSA alone, and showed that the gel fluorescence also arose from the porphyrin moiety (Fig. S40†).

## Application scenarios

We intended to demonstrate the biocompatibility and biospecificity of porphyrin bioconjugates constructed *via* β-fluoropyrrolyl-cysteine $S_NAr$ chemistry. In most cases, the biocompatibility and biological targetability of porphyrin was realized by nano-modification[13,51] or *meso*-bioconjugation.[20,21] We demonstrated the feasibility of porphyrin β-bioconjugates for the intracellular delivery of functional proteins, fluorescent imaging of sialoglycoproteins, caspase-3 detection, and cancer-selective photodynamic therapy, demonstrating the very attractive application potential of this methodology.

**Protein–polydisulfide (PDS) conjugation.** Cell-penetrating protein–polydisulfide (PDS) conjugates[52–54] showed great potential to aid the cytosolic delivery of functional proteins *via* thiol-mediated uptake.[55] For the synthesis of protein–PDS conjugates, *in situ* polymerization from a protein-of-interest (POI) surface-tethered cysteine ("grafting-from"; GF) displayed reduced steric hindrance and easier product purification than covalently linking a POI with a preformed PDS ("grafting-to"; GT). Given that porphyrin is widely used as a photosensitizer in photodynamic therapy (PDT), we provide a new methodology for the intracellular co-delivery of protein porphyrin drugs to combine protein therapy and phototheranostics. Although previous work reported porphyrin–PDS by synthesizing porphyrin *meso*-modified lipoic acid, the method was carried out in organic solvents, which was not compatible with biomolecules such as proteins, and could not induce NIR absorption by porphyrin after bioconjugation.[56]

In this work, we prepared protein–PDS conjugates with the cysteine-initiated cryo-ring-opening polymerization (cryo-ROP) of 1,2-dithiolanes (Fig. 5a, see details in the "Methods" part of ESI†).[48] After EGFP was mixed with lipoic acid (LA, 100 mM) at −30 °C, excess $\mathbf{P_{13}}$ or **IAA** was then added to cap the terminal free thiol, generating the protein–PDS conjugate denoted $\mathbf{P_{13}}$**-EGFP-PDS** or **IAA-EGFP-PDS**, respectively. CBB-stained non-reducing SDS-PAGE analysis (Fig. 5b) indicated that 76% and 54% of EGFP were converted into $\mathbf{P_{13}}$**-EGFP-PDS** and **IAA-EGFP-PDS**, respectively. Subsequently, we tested the cell-penetrating ability of $\mathbf{P_{13}}$**-EGFP-PDS** by incubating living HeLa cells with EGFP(i), $\mathbf{P_{13}}$**-EGFP** (ii), or $\mathbf{P_{13}}$**-EGFP-PDS** (iii) at pH 7.4. We observed pervasive and intense intracellular fluorescence in $\mathbf{P_{13}}$**-EGFP-PDS**-treated HeLa cells (Fig. 5c, iii), using confocal laser scanning microscopy. In contrast, no fluorescence was observed after treatment with free EGFP (Fig. 5c, i) or $\mathbf{P_{13}}$**-EGFP** (Fig. 5c, ii), revealing the good cell-penetrating capability of $\mathbf{P_{13}}$**-EGFP-PDS**.[48]

**Fluorescent imaging of sialoglycoproteins.** Generally, the porphyrin conjugates described here make possible the fluorescent labeling of biomolecules or biomarkers using unnatural metabolic precursors or a biotinylated antibody, which has not been achieved by porphyrin-based probes.[57] Glycans play essential functional roles in various biological processes, and metabolic glycan labeling (MGL) has emerged as a tool for analyzing glycans in cells and *in vivo*.[58] Streptavidin (Sav) fluorophore conjugates were often used due to their specific binding affinity with biotin, which can be artificially installed on glycoproteins.[57] Herein we prepared a β-Sav–porphyrin conjugate for MGL-based fluorescent imaging of sialoglycans (Fig. 6a). We introduced 2-iminothiolane (Traut's reagent) to convert the lysine residues of commercial Sav into free sulfhydryl groups in Tris buffer (pH 8.0); then used $\mathbf{P_{13}}$ as a porphyrin substrate. As shown in Fig. S41,† the main product was the $\mathbf{P_{13}}$**-Sav** conjugate containing four $\mathbf{P_{13}}$ moieties.

To visualize sialic acids *in vitro*, we used MGL technology to endow the nascent sialoglycans with azido groups[58] after incubation of HeLa cells with $Ac_4$ManNAz (50 μM) for 2 days. Next, to selectively modify sialic acids with biotin warheads, we applied copper-catalysed azide–alkyne cycloaddition (CuAAC)[59] between the biotin-PEG4-alkynyl group and the azido group on the cell surface after the cells were fixed (Fig. 6b). After washing and rinsing free biotin-PEG4-alkyne, $\mathbf{P_{13}}$**-Sav** was incubated with the HeLa cells, allowing the sialic acids to specifically recognize Sav-biotin. As shown in Fig. 6c, we observed intensive red fluorescence on the cell membranes, similar to previous studies using commercial Sav dyes.[57] As a control, a blank group without $Ac_4$ManNAz treatment showed no fluorescent signal. These results verified the feasibility of sialoglycoprotein labeling using $\mathbf{P_{13}}$**-Sav**, which is promising for MGL-assisted cancer phototheranostics.[58]

**Caspase-3 sensing *in vitro*.** Caspase-3 is a known key executor enzyme for regulating apoptosis signaling pathways.[60] Monitoring the activity of caspase-3 is important in studying apoptosis-related diseases. As several porphyrin-based sensors[61,62] displayed promising prospects in caspase-3-responsive photosensitizing, here we would like to investigate the feasibility of β-octafluoroporphyrin-based caspase-3 detection.

For this purpose, we designed a FRET (Förster resonance energy transfer) mechanism-based peptide probe $\mathbf{P_4}$**-k** (FITC-DEVDGC-$\mathbf{P_4}$),[63] which consisted of fluorescein (FITC) as the fluorescence reporter, a reactive polypeptide (DEVDGC) linker whose C-terminal amide bond can be specifically hydrolyzed by caspase-3,[64,65] and a porphyrin ($\mathbf{P_4}$) as the quencher of FITC (Fig. 7a). Treating $\mathbf{P_4}$**-k** (10 μM) with caspase-3 in PBS buffer gave strongly enhanced fluorescence, as shown in Fig. 7b (green line), while inhibiting the reactivity of caspase-3 using 5-[(*S*)-(+)-2(methoxymethyl)pyrrolidino]sulfonylisatin (MPS) showed no "turn-on" FITC fluorescence (blue line). Notably, the catalytic hydrolysis of $\mathbf{P_4}$**-k** by caspase-3 was also confirmed by HRMS, where the molecular ion peak with $m/z = 979.3045$ was detected, consistent with the calculated mass value ($[M + H]^+$) of FITC-DEVD.

To further demonstrate the specificity to caspase-3, we compared the fluorescence of $\mathbf{P_4}$**-k** in the presence of caspase-3, GSH, lysozyme, BSA, trypsin, DNAse, or caspase-7, respectively. As shown in Fig. 7c, only in the presence of caspase-3, did the fluorescence of $\mathbf{P_4}$**-k** show a 7-fold enhancement compared to the control. Note that the ratio of $F/F_0$ increased linearly along

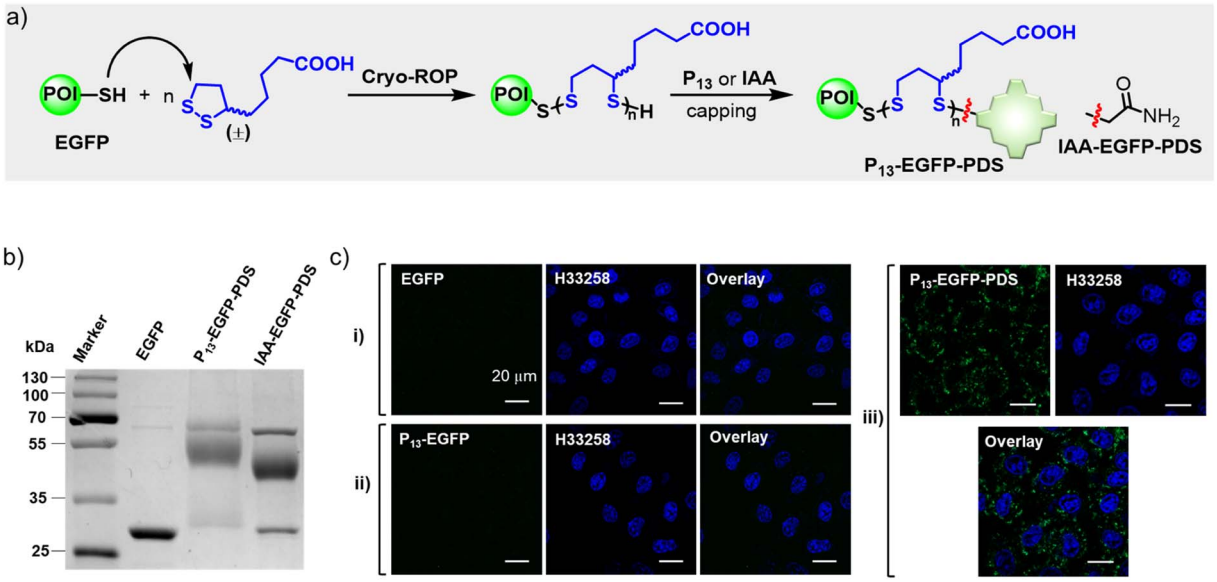


Fig. 5 (a) Schematic illustration of the synthesis of protein–polydisulfide (PDS) conjugates *via* cryo-ring-opening polymerization (cryo-ROP) of lipoic acid (LA). (b) CBB-stained non-reducing SDS-PAGE of cryo-ROP reaction mixture capped by $P_{13}$ or **IAA**. Conditions: pH = 7.0, EGFP concentration = 2.0 mg mL$^{-1}$, $[LA]_0$ = 100 mM, −30 °C, 2 h. (c) Fluorescence images of living HeLa cells treated with EGFP (250 nM, i), **$P_{13}$-EGFP** (250 nM, ii), or **$P_{13}$-EGFP-PDS** (250 nM, iii) at pH 7.4 for 1 h. $\lambda_{ex}$ = 450 nm; $\lambda_{em}$ = 525/50 nm bandpass filter.

with the concentration of caspase-3 (0–140 ng mL$^{-1}$, Fig. 7d), demonstrating a correlation between the fluorescence intensity and caspase-3. We subsequently performed an enzymatic assay in living HeLa cells to demonstrate the potential of **$P_4$-k** in detecting caspase-3 *in vitro*. As shown in Fig. 7e, when **$P_4$-k** was incubated, the weak green fluorescence of FITC was observed, while the fluorescence was remarkably enhanced (*ca.* 6-fold) upon the addition of staurosporine (STS), a widely used drug to induce apoptosis (Fig. 7e(ii), and f). Moreover, when MPS (5-[(*S*)-(+)-2-(methoxymethyl)pyrrolidino]sulfonylisatin) was adopted to inhibit caspase-3 activity, the fluorescence barely increased (Fig. 7e(iii) and f). This is consistent with Western blotting analysis for the expression of caspase-3 in HeLa cells with or without STS and MPS (Fig. 7g). Together, we demonstrated the capability of β-peptidyl porphyrins for detecting the activity of caspase-3 in living cells.

**Tumor-targeting *in vivo* phototheranostics.** Porphyrin-based photosensitizers have been widely used as phototheranostics that combine PDT and fluorescence imaging for tumors but usually lack specificity.[66] With this in mind, we prepared **$P_4$-f** by conjugating **$P_4$** with the $\alpha_v\beta_3$ integrin targeting peptide **f** (cRGDFC) and applied it in cancer-selective

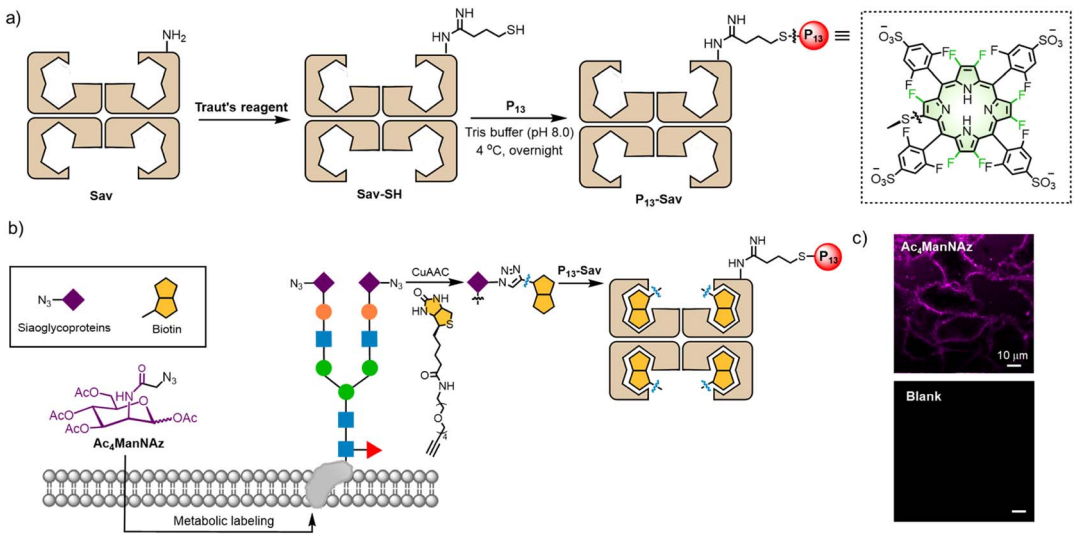


Fig. 6 Schematic illustration of (a) the synthesis of **$P_{13}$-Sav**. (b) $Ac_4$ManNAz metabolic labeling. (c) Fluorescence images of sialoglycoproteins using **$P_{13}$-Sav**. $\lambda_{ex}$ = 405 nm; $\lambda_{em}$ = 647 nm longpass filter. Scale bar: 10 μm.

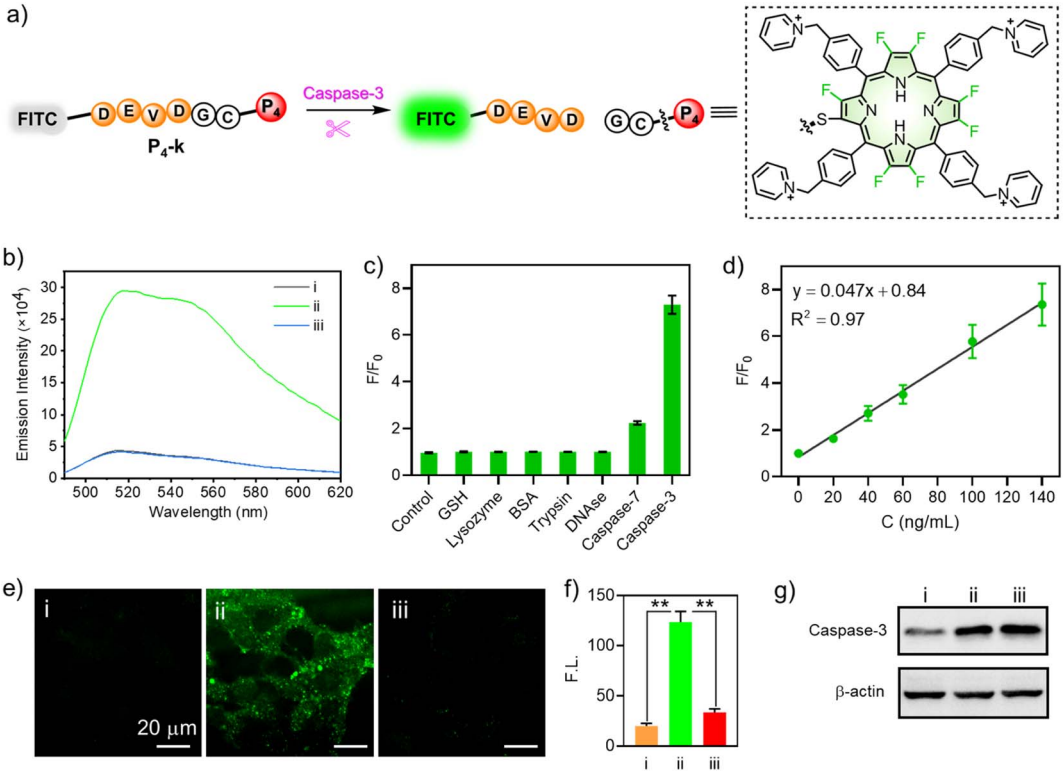


Fig. 7 (a) Schematic illustration of $P_4$-k as a fluorescent sensor for caspase-3. (b) Fluorescence spectra of $P_4$-k (10 μM) in PBS (pH 7.4) with selected treatments. $P_4$-k alone for i; caspase-3 + $P_4$-k for ii; inhibitor + caspase-3 + $P_4$-k for iii at 37 °C for 1 h. $\lambda_{ex}$ = 470 nm. (c) Fluorescence ratio ($F/F_0$) response of $P_4$-k to various species before ($F_0$) and after ($F$) incubation with various species for 1 h in PBS (1×, pH 7.4). The concentration of GSH is 10 mM. The concentrations of lysozyme, BSA, trypsin, and DNAse are all 1 μg mL$^{-1}$. The concentrations of caspase-7 and caspase-3 are 200 ng mL$^{-1}$. (d) Linear fitting curve of $F/F_0$ to the concentration of caspase-3 (0–140 ng mL$^{-1}$). $\lambda_{ex}$ = 470 nm. The reaction was conducted in PBS (1×, pH 7.4) at 37 °C for 1 h. (e) Fluorescence microscope images. $\lambda_{ex}$ = 488 nm; $\lambda_{em}$ = 525/50 nm bandpass filter. Scale bar: 20 μm. (f) Quantitative fluorescence intensity analysis of cell images in (e). (g) Expression level of caspase-3 of HeLa cells measured by Western blot assay. (i): HeLa cells were treated with $P_4$-k (10 μM) for 1 h. (ii): HeLa cells underwent induced apoptosis by STS (3 μM) for 2 h, and were then cultured with $P_4$-k (10 μM) for 1 h. (iii): HeLa cells were successively cultured with caspase-3 (10 μM) inhibitor and STS (3 μM) for 2 h, then with $P_4$-k (3 μM) for 1 h. (*$P$ < 0.05; **$P$ < 0.01).

PDT. To assess cell specificity, we conducted confocal fluorescence microscopy to track the intracellular fluorescence of **$P_4$**, **$P_4$-a**, and **$P_4$-f** in A549 human lung carcinoma cells with overexpression of integrin and MCF-7 human breast adenocarcinoma cells with low-expression of integrin (Fig. 8a).[67] For **$P_4$** and **$P_4$-a**, there was no apparent difference in fluorescence between MCF7 and A549 cells (Fig. 8a(i-ii)), while **$P_4$-f** showed *ca.* 3-fold higher fluorescence intensity in A549 cells than in MCF7 cells (Fig. 8a(iii)). Moreover, when we used iRGD (an RGD inhibitor) to block the integrin in A549, intracellular fluorescence in A549 incubated with **$P_4$-f** dropped to a similar level to that in MCF7 cells (Fig. 8a(iv)). These results suggested that **$P_4$-f** showed higher selectivity to A549 cells than MCF7, while **$P_4$** or **$P_4$-a** were non-specific and internalized by both cell lines.

Then we evaluated the feasibility of **$P_4$**, **$P_4$-a**, and **$P_4$-f** for *in vivo* PDT in A549 tumour mice by tail intravenous injection (Fig. 8c). The tumours were then subjected to irradiation (2 h post-injection, LED laser (400–700 nm), 100 mW cm$^{-2}$, 10 min). During 14 days of tumour growth monitoring (Fig. 8d), we observed significant inhibition of tumour growth in the "**$P_4$-f** + light" and "**$P_4$-a** + light" groups. In comparison, other groups ("**$P_4$**" or "**$P_4$** + light" groups) showed a minimal treatment effect. Note that tumour suppression was more effective in the "**$P_4$-f** + light" group than that in the "**$P_4$-a** + light" group due to the proven targeting ability of **$P_4$-f** toward A549 cells. At the end of the treatment, the tumours were dissected and photographed. As shown in Fig. 8e and f, the tumour volumes and weights in the "**$P_4$-f** + light" group were smaller than in the other groups. In particular, the tumour weights (0.0147 ± 0.0137 g) in the "**$P_4$-f** + light" group were much lower than those in the control (0.129 ± 0.0380 g) and the "**$P_4$-a** + light" groups (0.0320 ± 0.0175 g) due to the proven targeting ability of **$P_4$-f** toward A549 cells. The mice body weights showed no abnormal change in any treatment group compared to the control group (PBS), indicating that the three photosensitizers had no obvious systemic toxicity (Fig. S42†). This biosafety was further supported by hematoxylin and eosin (H & E) staining, where no damage was found in major organ tissues such as the heart, liver, spleen, or kidney (Fig. S43†). Therefore, these results revealed the perspective of novel β-peptidyl porphyrins as tumour-targeting phototheranostics combining PDT and imaging.

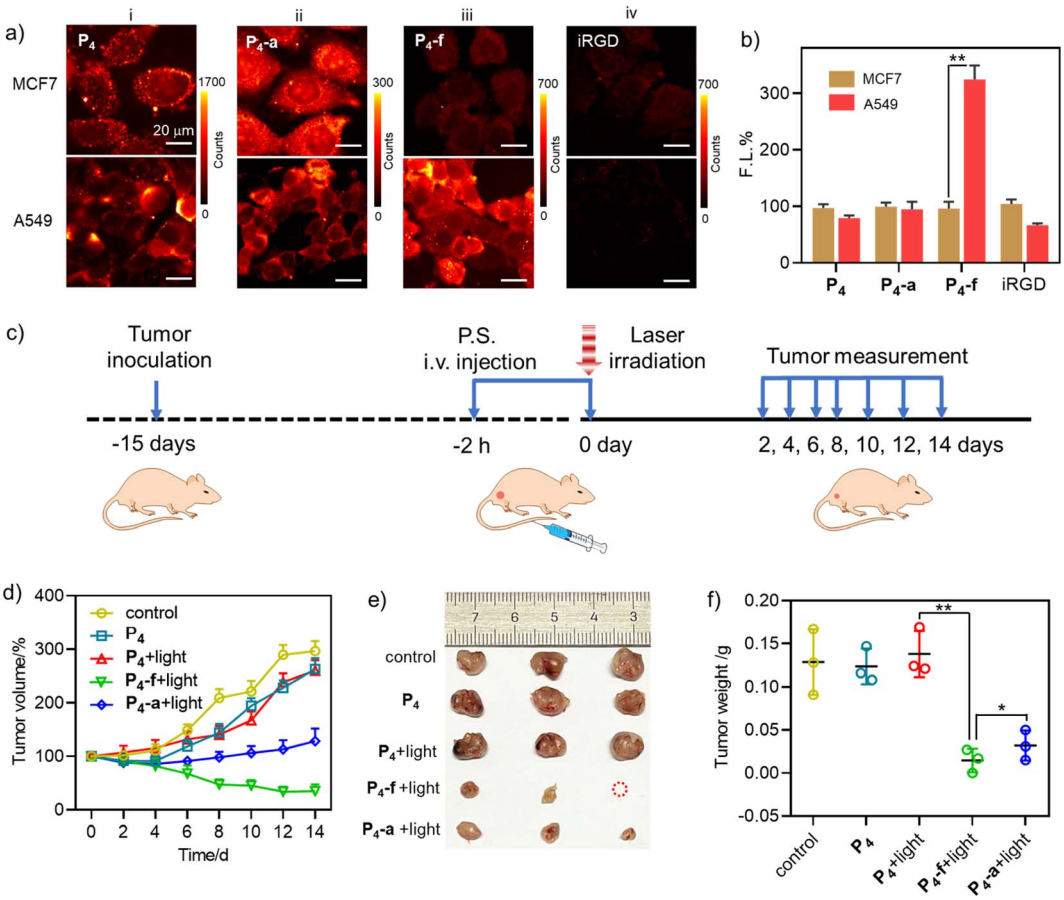


Fig. 8 (a) Fluorescence images of A549 and MCF7 cells after incubation with $P_4$ (8 μM, group i), $P_4$-**a** (8 μM, group ii), or $P_4$-**f** (8 μM, group iii) for 30 min. For group iv, the cells were incubated with iRGD (20 μM) for 1 h, then incubated with $P_4$-**f** (8 μM) for 30 min. $\lambda_{ex} = 405$ nm; $\lambda_{em} = 647$ nm longpass filter. (b) Quantitative fluorescence intensity analysis of fluorescence images of i–iv in (a). Red: A549 brown: MCF7. (*$P <$ 0.05; **$P < 0.01$). The fluorescence of each compound in groups i–iv in MCF7 was calculated as 100%, and the fluorescence intensity in A549 was expressed as a percentage of that in MCF7. (c) Schematic illustration of the treatment regimen. (d) Tumor volume variation curves for the mice in the "control (PBS)", "$P_4$", "$P_4$ + light", "$P_4$-**f** + light", and "$P_4$-**a** + light" groups during the treatment period ($n = 3$, mean ± SD). (e) Photographs of the tumours dissected from the mice in different groups. (f) Tumor weights of the mice in different groups at the end of treatment ($n = 3$, mean ± SD).

## Conclusions

We have developed an efficient and modular β-fluoropyrrolyl-cysteine $S_NAr$ preparation of irreversible peptide/protein–porphyrin bioconjugates. Due to the distinct electronic nature between fluorine and sulfur atoms, β-fluoropyrrolyl-cysteine $S_NAr$ chemistry represents a "two birds one stone" methodology that can not only covalently conjugate porphyrins with functional peptides/proteins but also induce intriguing photophysical properties, including facilitated ISC, red-shifted absorption, and increased singlet oxygen sensitization, which was highly favorable for phototheranostics. Moreover, these β-porphyrin bioconjugates have been applied in the intracellular delivery of EGFP, caspase-3 sensing *in vitro*, MGL, as well as *in vivo* tumor-targeting phototheranostics. β-Fluoropyrrolyl-cysteine $S_NAr$ chemistry provides unprecedented access to porphyrinic bioconjugates that enriches the repertoire of bioactive porphyrin. The present work highlights the promise of porphyrin bioconjugates as potential phototheranostics and the benefits that can accrue from manipulating the excited-state features of porphyrinoids. The fine-tuning of the structure and function achieved by the installation of β-sulfur atoms in porphyrin would also inspire research efforts to discover novel bioconjugation approaches based on other macrocycles and expand the functional range of small molecules for advanced materials and biomedical research.

## Author contributions

G.-Q. Jin and J.-L. Zhang planned and conducted the whole project experiments. J.-X. Wang and Y. Ning participated in chemical synthesis of β-octafluoroporphyrins. H. Zhang and J. Lu conducted the biological analysis and animal experiments. Y. Yao performed the theoretical calculations. J.-L. Zhang, S. Gao and H. Lu supervised the overall project. All authors contributed to the data analysis and the writing of the manuscript.

## Data availability

All data (NMR, HRMS, SDS-PAGE raw images, and Western blot raw images, *etc.*) have been provided in the main text and electronic ESI.†

## Conflicts of interest

The authors declare no competing financial interests. A Chinese patent (202111556065.4) has been applied that covers part of this work.

## Acknowledgements

We acknowledge financial support from the National Scientific Foundation of China (NSFC) (22131003, 21571007, 21621061, 21778002, and 21861162008). This work was supported by the High-performance Computing Platform of Peking University. This work was also supported by the Analytical Instrumentation Center of Peking University/the Center for Physicochemical Analysis and Measurements in ICCAS. All animal procedures were approved by the Institutional Animal Care and Use Committee of Sinoresearch (Beijing) Biotechnology Co., Ltd. (protocol number: 20211205).

## References

1 N. Krall, F. P. da Cruz, O. Boutureira and G. J. L. Bernardes, *Nat. Chem.*, 2016, **8**, 103–113.
2 S. J. Walsh, J. D. Bargh, F. M. Dannheim, A. R. Hanby, H. Seki, A. J. Counsell, X. Ou, E. Fowler, N. Ashman, Y. Takada, A. Isidro-Llobet, J. S. Parker, J. S. Carroll and D. R. Spring, *Chem. Soc. Rev.*, 2021, **50**, 1305–1353.
3 E. V. Vinogradova, C. Zhang, A. M. Spokoyny, B. L. Pentelute and S. L. Buchwald, *Nature*, 2015, **526**, 687–691.
4 S. Lin, X. Yang, S. Jia, M. Weeks Amy, M. Hornsby, S. Lee Peter, V. Nichiporuk Rita, T. Iavarone Anthony, A. Wells James, F. D. Toste and J. Chang Christopher, *Science*, 2017, **355**, 597–602.
5 Q. Luo, Y. Tao, W. Sheng, J. Lu and H. Wang, *Nat. Commun.*, 2019, **10**, 142.
6 B. Josephson, C. Fehl, P. G. Isenegger, S. Nadal, T. H. Wright, A. W. J. Poh, B. J. Bower, A. M. Giltrap, L. Chen, C. Batchelor-McAuley, G. Roper, O. Arisa, J. B. I. Sap, A. Kawamura, A. J. Baldwin, S. Mohammed, R. G. Compton, V. Gouverneur and B. G. Davis, *Nature*, 2020, **585**, 530–537.
7 Y. D. Gefei Li and J. Mo, Suwei Dong, Shin-ichiro Shoda and Xin-Shan Ye, *CCS Chem.*, 2021, **4**, 1930–1937.
8 R. Tessier, J. Ceballos, N. Guidotti, R. Simonet-Davin, B. Fierz and J. Waser, *Chem*, 2019, **5**, 2243–2263.
9 A. M.-H. Yip, C. K.-H. Lai, K. S.-M. Yiu and K. K.-W. Lo, *Angew. Chem., Int. Ed.*, 2022, **61**, e202116078.
10 S. Liu, C. Lin, Y. Xu, H. Luo, L. Peng, X. Zeng, H. Zheng, P. R. Chen and P. Zou, *Nat. Chem.*, 2021, **13**, 472–479.
11 H. Iwashita, E. Castillo, S. Messina Marco, A. Swanson Raymond and J. Chang Christopher, *Proc. Natl. Acad. Sci. U. S. A.*, 2021, **118**, e2018513118.
12 S. Singh, A. Aggarwal, N. V. S. D. K. Bhupathiraju, G. Arianna, K. Tiwari and C. M. Drain, *Chem. Rev.*, 2015, **115**, 10261–10306.
13 M. A. Rajora, J. W. H. Lou and G. Zheng, *Chem. Soc. Rev.*, 2017, **46**, 6433–6469.
14 Y. Ning, Y.-W. Liu, Z.-S. Yang, Y. Yao, L. Kang, J. L. Sessler and J.-L. Zhang, *J. Am. Chem. Soc.*, 2020, **142**, 6761–6768.
15 J. F. Arambula and J. L. Sessler, *Chem*, 2020, **6**, 1634–1651.
16 J.-Y. Liu, E. A. Ermilov, B. Röder and D. K. P. Ng, *J. Porphyrins Phthalocyanines*, 2013, **17**, 831–835.
17 N. M. Casellas, G. Dai, E. Y. Xue, M. Jesús Vicente-Arana, D. K. P. Ng, T. Torres and M. García-Iglesias, *Biomater. Sci.*, 2022, **10**, 3259–3267.
18 E. Stulz, *Acc. Chem. Res.*, 2017, **50**, 823–831.
19 P. Pathak, W. Yao, K. D. Hook, R. Vik, F. R. Winnerdy, J. Q. Brown, B. C. Gibb, Z. F. Pursell, A. T. Phan and J. Jayawickramarajah, *J. Am. Chem. Soc.*, 2019, **141**, 12582–12591.
20 F. Biscaglia and M. Gobbo, *Pept. Sci.*, 2018, **110**, e24038.
21 J. Sandland and R. W. Boyle, *Bioconjugate Chem.*, 2019, **30**, 975–993.
22 P. M. R. Pereira, S. Silva, M. Bispo, M. Zuzarte, C. Gomes, H. Girão, J. A. S. Cavaleiro, C. A. F. Ribeiro, J. P. C. Tomé and R. Fernandes, *Bioconjugate Chem.*, 2016, **27**, 2762–2769.
23 P. Ochtrop and C. P. R. Hackenberger, *Curr. Opin. Chem. Biol.*, 2020, **58**, 28–36.
24 H. Seki, S. J. Walsh, J. D. Bargh, J. S. Parker, J. Carroll and D. R. Spring, *Chem. Sci.*, 2021, **12**, 9060–9068.
25 L. Xu, M. J. S. A. Silva, P. M. P. Gois, S. L. Kuan and T. Weil, *Chem. Sci.*, 2021, **12**, 13321–13330.
26 Y. Zhang, C. Zang, G. An, M. Shang, Z. Cui, G. Chen, Z. Xi and C. Zhou, *Nat. Commun.*, 2020, **11**, 1015.
27 E. A. Hoyt, P. M. S. D. Cal, B. L. Oliveira and G. J. L. Bernardes, *Nat. Rev. Chem.*, 2019, **3**, 147–171.
28 H. Liu, W. Song, S. Zhang, K. S. Chan, Z. Guo and Z. Shen, *Chem. Sci.*, 2020, **11**, 8495–8501.
29 C. Ma, Z. Xia, M. D. Sacco, Y. Hu, J. A. Townsend, X. Meng, J. Choza, H. Tan, J. Jang, M. V. Gongora, X. Zhang, F. Zhang, Y. Xiang, M. T. Marty, Y. Chen and J. Wang, *J. Am. Chem. Soc.*, 2021, **143**, 20697–20709.
30 B. Bernardim, M. J. Matos, X. Ferhati, I. Compañón, A. Guerreiro, P. Akkapeddi, A. C. B. Burtoloso, G. Jiménez-Osés, F. Corzana and G. J. L. Bernardes, *Nat. Protoc.*, 2019, **14**, 86–99.
31 C. Zhang, M. Welborn, T. Zhu, N. J. Yang, M. S. Santos, T. Van Voorhis and B. L. Pentelute, *Nat. Chem.*, 2016, **8**, 120–128.
32 S. Kalhor-Monfared, M. R. Jafari, J. T. Patterson, P. I. Kitov, J. J. Dwyer, J. M. Nuss and R. Derda, *Chem. Sci.*, 2016, **7**, 3785–3790.
33 A. M. Embaby, S. Schoffelen, C. Kofoed, M. Meldal and F. Diness, *Angew. Chem., Int. Ed.*, 2018, **57**, 8022–8026.
34 T. Tsunemi, S. J. Bernardino, A. Mendoza, C. G. Jones and P. G. Harran, *Angew. Chem., Int. Ed.*, 2020, **59**, 674–678.
35 D. O'Hagan, *Chem. Soc. Rev.*, 2008, **37**, 308–319.
36 J. Gonzales, N. V. S. D. K. Bhupathiraju, W. Perea, H. Chu, N. Berisha, V. Bueno, N. Dodic, J. Rozenberg,

N. L. Greenbaum and C. M. Drain, *Chem. Commun.*, 2017, **53**, 3773–3776.
37 J. Tang, M. A. Robichaux, K.-L. Wu, J. Pei, N. T. Nguyen, Y. Zhou, T. G. Wensel and H. Xiao, *J. Am. Chem. Soc.*, 2019, **141**, 14699–14706.
38 V.-N. Nguyen, S. Qi, S. Kim, N. Kwon, G. Kim, Y. Yim, S. Park and J. Yoon, *J. Am. Chem. Soc.*, 2019, **141**, 16243–16248.
39 V.-N. Nguyen, Y. Yan, J. Zhao and J. Yoon, *Acc. Chem. Res.*, 2021, **54**, 207–220.
40 G. K. Balendiran, R. Dabur and D. Fraser, *Cell Biochem. Funct.*, 2004, **22**, 343–352.
41 N. V. S. D. K. Bhupathiraju, W. Rizvi, J. D. Batteas and C. M. Drain, *Org. Biomol. Chem.*, 2016, **14**, 389–408.
42 J. Kvíčala, M. Beneš, O. Paleta and V. Král, *J. Fluorine Chem.*, 2010, **131**, 1327–1337.
43 K. Ding, L. Wang, J. Zhu, D. He, Y. Huang, W. Zhang, Z. Wang, A. Qin, J. Hou and B. Z. Tang, *ACS Nano*, 2022, **16**, 7535–7546.
44 X. Meng, Y. Yi, Y. Meng, G. Lv, X. Jiang, Y. Wu, W. Yang, Y. Yao, H. Xu and W. Bu, *ACS Nano*, 2022, **16**, 4217–4227.
45 J. Tang, L. Wang, A. Loredo, C. Cole and H. Xiao, *Chem. Sci.*, 2020, **11**, 6701–6708.
46 V. V. Rostovtsev, L. G. Green, V. V. Fokin and K. B. Sharpless, *Angew. Chem., Int. Ed.*, 2002, **41**, 2596–2599.
47 N. J. Agard, J. A. Prescher and C. R. Bertozzi, *J. Am. Chem. Soc.*, 2004, **126**, 15046–15047.
48 J. Lu, H. Wang, Z. Tian, Y. Hou and H. Lu, *J. Am. Chem. Soc.*, 2020, **142**, 1217–1221.
49 H. Choi, M. Kim, J. Jang and S. Hong, *Angew. Chem., Int. Ed.*, 2020, **59**, 22514–22522.
50 Q. Chen and Z. Liu, *Adv. Mater.*, 2016, **28**, 10557–10566.
51 J. Mao, Z. Xu and W. Lin, *Curr. Opin. Chem. Eng.*, 2022, **38**, 100871.
52 G. Gasparini, E.-K. Bang, G. Molinard, D. V. Tulumello, S. Ward, S. O. Kelley, A. Roux, N. Sakai and S. Matile, *J. Am. Chem. Soc.*, 2014, **136**, 6069–6074.
53 J. Fu, C. Yu, L. Li and S. Q. Yao, *J. Am. Chem. Soc.*, 2015, **137**, 12153–12160.
54 H. Wang, Y. Hu, Y. Wang, J. Lu and H. Lu, *Giant*, 2021, **5**, 100040.
55 Q. Laurent, R. Martinent, B. Lim, A.-T. Pham, T. Kato, J. López-Andarias, N. Sakai and S. Matile, *JACS Au*, 2021, **1**, 710–728.
56 J. W. Trzciński, L. Morillas-Becerril, S. Scarpa, M. Tannorella, F. Muraca, F. Rastrelli, C. Castellani, M. Fedrigo, A. Angelini, R. Tavano, E. Papini and F. Mancin, *Biomacromolecules*, 2021, **22**, 467–480.
57 D.-e. Sun, X. Fan, Y. Shi, H. Zhang, Z. Huang, B. Cheng, Q. Tang, W. Li, Y. Zhu, J. Bai, W. Liu, Y. Li, X. Wang, X. Lei and X. Chen, *Nat. Methods*, 2021, **18**, 107–113.
58 B. Cheng, Q. Tang, C. Zhang and X. Chen, *Annu. Rev. Anal. Chem.*, 2021, **14**, 363–387.
59 C. Besanceney-Webler, H. Jiang, T. Zheng, L. Feng, D. Soriano del Amo, W. Wang, L. M. Klivansky, F. L. Marlow, Y. Liu and P. Wu, *Angew. Chem., Int. Ed.*, 2011, **50**, 8051–8056.
60 A. G. Porter and R. U. Jänicke, *Cell Death Differ.*, 1999, **6**, 99–104.
61 J. F. Lovell, M. W. Chan, Q. Qi, J. Chen and G. Zheng, *J. Am. Chem. Soc.*, 2011, **133**, 18580–18582.
62 L. Zhang, J. Lei, F. Ma, P. Ling, J. Liu and H. Ju, *Chem. Commun.*, 2015, **51**, 10831–10834.
63 P. Pyykkö, *Angew. Chem., Int. Ed.*, 2006, **45**, 28–29.
64 D. Ye, A. J. Shuhendler, L. Cui, L. Tong, S. S. Tee, G. Tikhomirov, D. W. Felsher and J. Rao, *Nat. Chem.*, 2014, **6**, 519–526.
65 Y. Jin, K. Xu, Y. Huang, H. Zhong and R. Zhao, *Anal. Chem.*, 2021, **93**, 2045–2052.
66 G. I. Vargas-Zúñiga, H. S. Kim, M. Li, J. L. Sessler and J. S. Kim, *J. Porphyrins Phthalocyanines*, 2021, **25**, 773–793.
67 S. Y. Y. Ha, R. C. H. Wong, C. T. T. Wong and D. K. P. Ng, *Eur. J. Med. Chem.*, 2019, **174**, 56–65.